JOURNAL OF CATALYSIS 153, 158–164 (1995)

The Effect of Subsurface Oxygen on the Desorption Kinetics of Propylene from Ag(110)

Jacquelyn Pawela-Crew and Robert J. Madix

Department of Chemical Engineering, Stanford University, Stanford, California 94305

Received October 7, 1994; revised January 9, 1995

The effect of subsurface oxygen on the desorption of π-bonded propylene from Ag(110) was studied using temperature programmed desorption and x-ray photoelectron spectroscopy. The kinetic parameters for propylene desorption from Ag(110) without subsurface oxygen were compared to those for propylene desorption from Ag(110) when the subsurface region was saturated with oxygen. In the limit of zero coverage the activation energy and preexponential factor for propylene desorption from Ag(110) with subsurface oxygen is equal to the activation energy and preexponential factor for propylene desorption from Ag(110) without subsurface oxygen (E_0 = 12.7 ± 0.6 kcal/mol, $\nu = 1.2 \times 10^{16}$ s^{-1}). On both Ag(110) surfaces, with and without subsurface oxygen, the activation energy for desorption decreases as the propylene coverage increases indicative of weak repulsive interactions. The difference in the lateral interaction energy for propylene on the two surfaces is within the experimental uncertainty. Subsurface oxygen apparently does not affect the kinetic parameters even for the desorption of a weakly π-bound species from Ag(110), even though surface oxygen is known to strengthen such bonds. © 1995 Academic Press, Inc.

1. INTRODUCTION

The role of subsurface oxygen in catalysis is not well understood. Many have concluded that adsorbed atomic oxygen and subsurface oxygen are necessary in ethylene epoxidation reactions on Ag(110) (1–3). Hartree–Fock–Slater cluster calculations (3) predict that subsurface oxygen weakens the chemisorbed oxygen–silver bond, thereby facilitating atomic oxygen transfer to ethylene (3). However, Campbell *et al.* (4) propose that subsurface oxygen is not necessary in the epoxidation reaction. Furthermore, NEXAFS studies show that subsurface oxygen neither alters the orientation nor detectably shifts the position of the energies of the lowest unoccupied orbitals of chemisorbed molecular oxygen on Ag(110) (5).

The presence of chemisorbed surface oxygen atoms is known to increase the sticking probability of propylene adsorbed at 140 K on Ag(110) (6). It has also been reported that oxygen strengthens adsorption for several oxygen-containing molecules on the Ag(110) surface (7–9). It is hypothesized (10) that the highly electronegative oxygen atoms withdraw electrons from neighboring silver atoms at the surface, leading to electron-deficient silver atoms which act as Lewis acid sites for electron donors, resulting in a stronger adsorbate–silver bond. It has been suggested that in the case of olefins such as ethylene and propylene this interaction most likely occurs with the olefin π system (6). Studies have shown that for propylene oxidation, combustion occurs via an acid–base reaction with the chemisorbed atomic oxygen (6, 11). In addition, it has been demonstrated that electrophilic attack by O(a) on the olefinic bond is a crucial step in epoxidation (12, 13). Propylene adsorption on the oxygen-covered Ag(110) surface has been studied previously, but it was assumed that the effect of subsurface oxygen was negligible in this reaction (6). In this study we show that *subsurface* oxygen does not affect even the weak bonding of alkenes to the silver surface atoms. Hereafter we refer to subsurface oxygen as O(s).

The effect of subsurface oxygen on the activation energy, preexponential factor, and lateral interaction energy for propylene desorption from Ag(110) was investigated using three different methods to evaluate temperature-programmed desorption profiles, including leading edge analysis, Redhead analysis, and isotherms. The second virial coefficient for the 2D adsorbed phase was calculated using the quasiequilibrium assumption from the desorption isotherms, in which the coverage and rate of desorption are related to the chemical potential which is expressed in terms of a virial expansion (14–16). A complete derivation of this can be found in the work of Kevan *et al.*, in which the 2D adsorbed phase second virial coefficient for methane on Ag(110) (14), CO on Cu(001) (15), CO on Cu(011), NH_3 on Cu(001), and ND_3 on Cu(001) (16) were calculated. These studies have shown that the second virial coefficient for CH_4 on Ag(110) at 57.5 K and 59.5 K are −94 Å^2 and −80 Å^2 (14), respectively; CO on Cu(011) and CO on Cu(001) (17) at 75–79 K also exhibit negative values of B_2, indicating that attractive interac-

0021-9517/95 $6.00

tions predominate among these adsorbed molecules. The NH_3/Cu(001) and ND_3/Cu(001) systems were found to have positive values of B_2, indicating repulsive interactions between 200 and 230 K.

We report here that subsurface oxygen does not affect the kinetic parameters for propylene desorption on Ag(110). The activation energy and preexponential factor are equivalent in both systems, and the lateral interaction energies differ by only by about 1 kcal/mol. The virial analysis yields positive second virial coefficients in agreement with the overall behavior of the desorption peaks as a function of coverage.

2. EXPERIMENTAL

Temperature programmed desorption (TPD) and x-ray photoelectron spectroscopy (XPS) were carried out in an ultra-high-vacuum chamber previously described (18). The crystal was placed in contact with a liquid-nitrogen-filled cooper block and could be cooled to 100 K. A tungsten filament mounted behind the crystal was used to radiatively heat the crystal. The temperature of the crystal was monitored using a chromel–alumel thermocouple pressed into a hole in the crystal. TPD data were acquired using a UTI 100C mass spectrometer interfaced to an IBM XT computer. The computer program used allowed up to 10 masses to be scanned simultaneously.

The Ag(110) surface was cleaned by argon-ion bombardment at 300 K followed by annealing to 760 K until no impurities were detected using Auger electron spectroscopy. Residual surface carbon was removed by adsorption/desorption cycles in which 24 L (1 L = 10^{-6} Torr · s) of oxygen was dosed at 300 K. The oxygen cleaning cycles continued until the integrated temperature programmed reaction yield of CO_2 produced from carbon oxidation was less than 5% of the yield of the desorbed oxygen. The subsurface oxygen was removed by argon ion bombardment at 300 K followed by annealing to 760 K. A series of adsorption/desorption cycles in which 0.5 ML O_2 was dosed at 300 K and heated to 700 K were conducted to increase the amount of subsurface oxygen.

The relative coverage of propylene was determined using XPS by utilizing the fact that the photoelectron intensity in the XPS peak is directly proportional to the coverage (19). A known surface coverage was used as a standard to determine the XPS signal per monolayer (ML) of adsorbate atoms, where one ML is defined as the number of silver atoms in the first layer of the Ag(110) surface (8.5×10^{14} cm^{-2}). The number of carbon atoms present in an adsorbed layer was calculated from the area of the C(1*s*) XPS peak using the measured relative sensitivity value of 3.31 ± 0.2 for oxygen and carbon. Details of the XPS coverage calibration procedure are published elsewhere (20).

The C (1*s*) and O (1*s*) peaks were normalized to the Ag ($3d_{5/2}$) peak to account for any drift during experiments or changes in signal intensity due to modifications in the crystal position relative to the x-ray source. The Ag ($3d_{5/2}$) peak was recorded prior to each C (1*s*) and O (1*s*) spectra. For all the XPS spectra, 256 scans (44 min) were collected at 300 K and signal averaged at an analyzer pass energy of 50 eV. The error in the C (1*s*) binding energy was calculated in a previous study to be ±0.3 eV (21).

Propylene (99.0% purity) was obtained from Liquid Carbonic; oxygen (99.998% min. purity) and argon (99.995% min. purity) were obtained from Matheson Gas Products. These gases were used without further purification.

The leading edge method (22, 23) was used in this study to determine the activation energy for desorption, the preexponential factor, and the lateral interaction energy for propylene desorption from Ag(110) with and without O(s). A small temperature interval in which T and θ remain relatively constant ($\Delta\theta/\theta = 0.03$) was selected at the low-temperature, high-coverage side of the TPD curve. An Arrhenius plot ($\ln(r)$ versus $1/T$) of this interval yielded a straight line with slope $-E(\theta)/R$ and intercept equal to $\ln(\nu) + n \ln(\theta)$, where n, the reaction order, was assumed to be one. The value of ν was calculated from the intercept of the Arrhenius plot at a particular value of θ. The slope of this line was taken for coverages up to 3% of the total initial coverage. Only ln(rate) values larger than −4.0 were accepted in the analysis; this limit corresponds to the minimum resolution of the analog/digital converter. Details regarding the leading edge analysis are published elsewhere (20). The global coverage dependence of the activation energy was taken as $E = E_0 + W\theta$, where E_0 is the activation energy in the limit of zero coverage and W is the lateral interaction energy.

The activation energy was also calculated using the Redhead peak maximum method and compared to the values obtained from the leading edge analysis, using (31),

$$E = RT_d(\ln(\nu T_d/\beta) - 3.46), \qquad [1]$$

where T_d is the peak temperature for desorption, ν is the preexponential factor, and β the heating rate (9 K/s with O(s), 6 K/s without O(s)). The value of ν (10^{15} s^{-1}) used in the Redhead calculation was obtained from the leading edge analysis. The isothermal analysis is discussed below.

3. RESULTS

3.1. X-Ray Photoelectron Spectroscopy

The chemisorbed oxygen O (1*s*) peak and the subsurface oxygen O (1*s*) peak were observed at 528 eV and 531 eV, respectively. Figure 1 indicates that the low energy

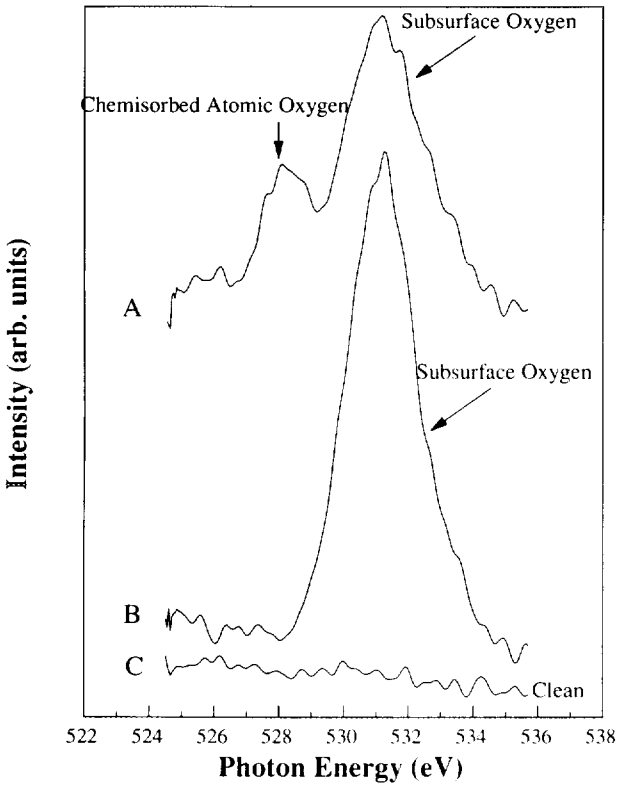

FIG. 1. XPS spectra of subsurface oxygen on Ag(110) (A) after several adsorption/desorption cycles in which oxygen was dosed at 300 K and the surface was heated to 690 K. In the final cycle oxygen was dosed at 300 K and the surface was not heated. (B) After several adsorption/desorption cycles in which oxygen was dosed at 300 K and the surface was heated to 690 K. In the final cycle oxygen was dosed to 300 K and the surface was heated to 690 K. (C) After sputtering for 30 min at 300 K and annealing to 760 K.

peak at 528 eV observed at ~280 K is no longer observed after the surface is heated to 595 K (curve b). This result suggests that the oxygen corresponding to the low energy peak (528 eV) recombines and desorbs as molecular oxygen, a reaction known to occur at 590 K (24). In addition, the low energy oxygen state at 528 eV was found to combine with adsorbed carbon and desorb as CO_2 at 450 K and O_2 at 590 K. The O (1*s*) peak at 531 eV is not reactive to C(a) and does not desorb as CO_2 or O_2 below 800 K. The reactivity and desorption temperature of the O (1*s*) peak at 528 eV indicate that this peak represents chemisorbed atomic oxygen whereas the peak at 531 eV is attributed to oxygen located in the subsurface region.

The assignment of the low energy peak at 528 eV to chemisorbed surface atomic oxygen and the high energy peak (531 eV) to subsurface oxygen is in agreement with previous XPS subsurface oxygen studies on silver (25–27). Joyner and Roberts (25) observed a chemisorbed atomic oxygen peak at 528.3 eV and a subsurface oxygen peak at 530.3 eV. These assignments were based on both a study of the angular dependence of the O (1*s*) spectra and the observation that the high energy peak is unreactive to C(a), while no C(a) is observed in the presence of the low energy peak. In addition, Campbell *et al.* (28) observed a subsurface oxygen peak at 528.5 eV and a chemisorbed atomic surface oxygen peak at 528.1 eV. In a similar study, Barteau (27) assigned the XPS peaks observed at 531.2 eV and 529.2 eV to subsurface oxygen and chemisorbed atomic oxygen, respectively.

The XPS O (1*s*) peak intensity of 531 eV was used to quantify the amount of O(s) relative to a saturated chemisorbed atomic oxygen layer (0.5 ML). A $p(2 \times 1)$ LEED pattern was observed prior to acquisition of the XPS spectra in Fig. 1, curve A. Previous studies (27, 29) have found that a $p(2 \times 1)$ LEED pattern is observed at an oxygen coverage of 0.5 ML (saturation coverage). These studies verify the assumption that the peak at 528 eV in Fig. 1 represents 0.5 ML chemisorbed atomic oxygen. The subsurface oxygen peak at 531 eV in curve A is 3.4 times larger than the chemisorbed atomic oxygen peak (528 eV). The subsurface oxygen peak in spectrum B is 4.75 times greater than the chemisorbed atomic oxygen peak in spectrum A, corresponding to approximately the equivalent of 2.5 ML of subsurface oxygen. The distribution of O(s) below the surface can not be deduced with these XPS data. Although the XPS sampling depth of the O (1*s*) electrons is approximately six atomic layers, it is not certain how many layers below the surface the subsurface oxygen extends. However, since the XPS signal for subsurface oxygen did not decrease when surface oxygen was desorbed, and the subsurface oxygen readily exchanged with isotopically labeled surface oxygen, it appears that subsurface oxygen was not depleted from the near-surface region by the treatment employed to desorb surface oxygen.

3.2. Temperature Programmed Desorption

The peak temperature for the desorption of propylene on Ag(110) both with and without O(s) shifts downward as the coverage increases. The temperature-programmed desorption spectra from Ag(110) without O(s) are shown in Fig. 2 for coverages ranging from 0.04 ML to 0.74 ML. The desorption temperature ranges from 170 to 155 K in this coverage region. Figure 3 shows the desorption peaks from Ag(110) with subsurface oxygen, which range from 168 to 150 K for coverages between 0.06 and 0.71 ML. The rate of desorption and the peak temperature are lower for the surface without subsurface oxygen independent of any kinetic differences in the rates of desorption, since the heating rate used was lower (30). Even without correcting for differences in heating rates, it is clear that the desorption energies do not differ appreciably on the two

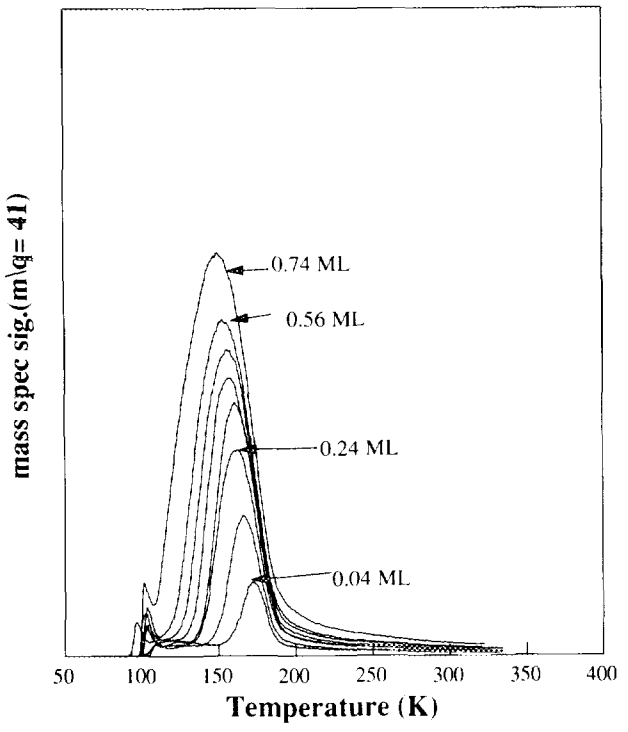

FIG. 2. Temperature programmed desorption spectra of propylene on Ag(110) without O(s). Propylene was dosed at various coverages at 100 K.

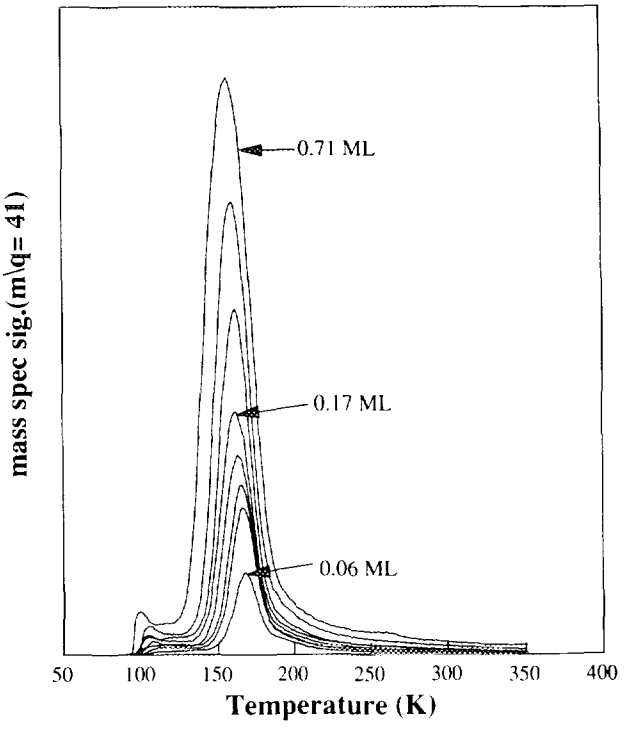

FIG. 3. Temperature-programmed desorption spectra of propylene on Ag(110) with O(s). Propylene was dosed at various coverages at 100 K.

surfaces, since the difference in peak temperatures differ by only about 5 K at comparable coverages. The TPD data from the two surfaces is compared directly in Fig. 4.

The leading edge analysis yields nearly equal values of E_0 and ν for propylene desorption from Ag(110) with and without O(s); however, the calculated values of W appear somewhat different (Fig. 5). Linear regression of the data gives $E_0 = 12.7 \pm 0.6$ kcal/mol and $W = -9.0 \pm 1.2$ kcal for desorption of propylene from Ag(110) without O(s) and $E_0 = 11.7 \pm 0.4$ kcal/mol and $W = -3.1 \pm 0.5$ kcal from the surface with O(s), where E_0 is the activation energy at $\theta_{\text{propylene}} = 0$ and W is the lateral interaction energy. For the system without O(s), $\nu = 7 \pm 2 \times 10^{15}$ sec^{-1}; with O(s) $\nu = 3 \pm 2 \times 10^{15}$ s^{-1}. Some interference from the low-temperature desorption state was also present in the low coverage TPD on the surface without O(s). For this reason the magnitude of W obtained from the threshold analysis for the surface without O(s) is somewhat uncertain.

The activation energy for propylene desorption from Ag(110) *with* O(s) calculated using the Redhead method is in agreement with the leading edge values. Using Eq. [1] from the Redhead analysis and a preexponential value of 10^{15} s^{-1}, we obtain $E = 10.1 \pm 0.5$ kcal/mol at $T_d = 150$ K and $E = 11.9 \pm 1.0$ kcal/mol at $T_d = 175$ K. The higher of these desorption temperatures corresponds to

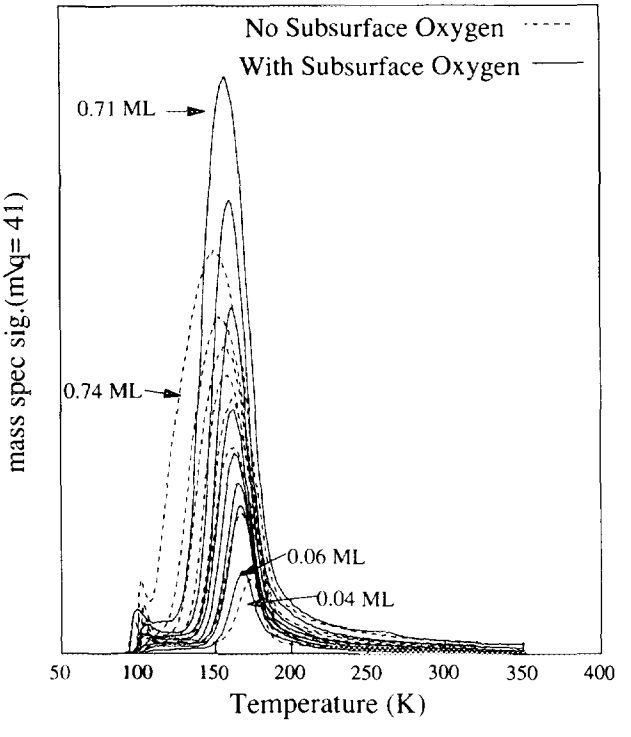

FIG. 4. TPD spectra from Figs. 2 and 3. Propylene on Ag(110) with subsurface oxygen TPD peaks are solid lines and propylene on Ag(110) without subsurface oxygen spectra are represented by dashed lines.

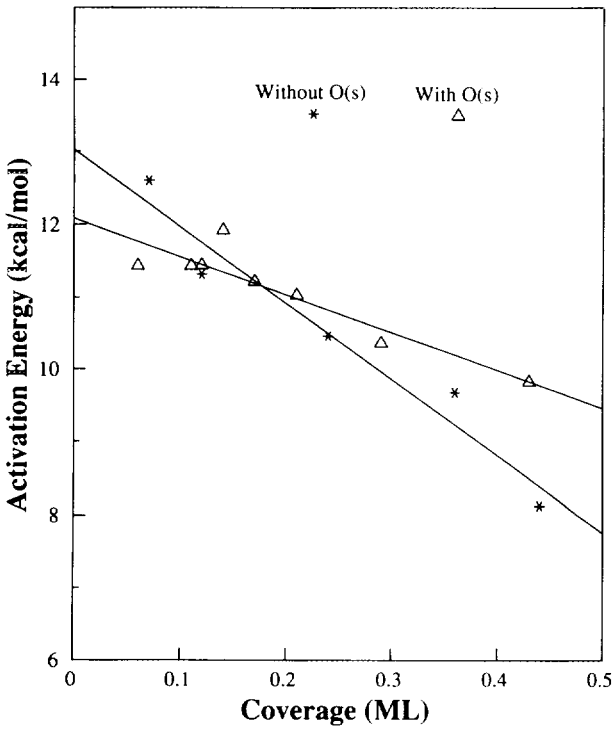

FIG. 5. Results for activation energy as a function of coverage. The data points were calculated using the leading edge analysis. The slope of the linear regressed line is equal to the lateral interaction energy, W.

the lowest coverage, therefore the value obtained at this temperature should be close to the E_0 value obtained from the leading edge analysis, as it is. In addition, at T_d = 150 K, $\theta_{propylene}$ = 0.64 ML, which gives E = 10.1 ± 0.5 kcal/mol using the leading edge method. This value agrees with the value of E calculated at T_d = 150 K from the Redhead analysis. Given that the Redhead analysis results agree with the leading edge results at the highest and lowest propylene coverages, it is clear that the interaction energy calculated from the Redhead method is within experimental error of the value obtained from the leading edge analysis for the surface with O(s).

The Redhead calculations agree with the leading edge results obtained in the low coverage region for the system *without* O(s) but disagree with the leading edge results in the high coverage region. For example, at T = 170 K (θ = 0.07 ML), E = 12.4 ± 1.2 kcal/mol using the Redhead analysis compared to 12.7 ± 0.6 for the value of E_0 obtained in the low-coverage region by the threshold analysis. The two methods do not agree at higher coverage, however. At θ = 0.5 ML the leading edge analysis gives E = 8.2 ± 0.5 kcal/mol, compared to E = 11.2 ± 1.2 kcal/mol using the Redhead method (T = 155 K). We attribute this difference primarily to the interference from the low temperature desorption state in the leading edge analysis, since this difference does not persist in the isothermal treatment (see below). The results from the leading edge analysis and the Redhead peak maximum method are summarized in Table 1.

To estimate the accuracy of the lateral interaction energy values calculated from the other methods, W was calculated by computing the second virial coefficient, B_2, obtained from temperature programmed desorption (20). Plots of the desorption isotherms, integrated to obtain relative coverages and thereby $\ln(r_d/\theta)$ vs θ, at various temperatures are shown for propylene on Ag(110) with and without O(s) in Figs. 6 and 7. According to the following expression derived from the quasi-equilibrium approximation and the virial equation of state for the rate of desorption (20), the slope of these isotherms is proportional to B_2.

$$\frac{r_d}{\theta N_m} = \frac{\sigma(\theta, T)\,\mathrm{Aq_i}k_bT}{hQ_1\Lambda^2}\exp\left(\frac{-E_0}{k_bT}\right)\exp\left(\sum_{j\geq 1}\frac{j+1}{j}B_{j+1}\left(\frac{N_m}{A}\theta\right)^j\right), \quad [2]$$

where (N_m/A) is equal to the number of adsorption sites per unit area of the Ag(110) surface (8.47 × 10^{14} atoms/cm^2), σ(T, θ) is the thermally averaged sticking coefficient, A is the area of adsorption sites per unit area of

TABLE 1

Leading Edge and Redhead Peak Maximum Analysis Results

	Leading edge analysis			Redhead peak maximum analysis	
Propylene on Ag(110)	E_0 (kcal/mol)	W (kcal/mol)	ν (sec^{-1})	Temp. (K)	E_0 (kcal/mol)
With O(s)	11.7 ± 0.4	−3.1 ± 0.5	1.6 × 10^{16}	175 K	11.9 ± 1.0
				150 K	10.1 ± 0.5
Without O(s)	12.7 ± 0.6	−9.0 ± 1.2	2.0 × 10^{16}	170 K	12.4 ± 1.2
				155 K	11.2 ± 1.2

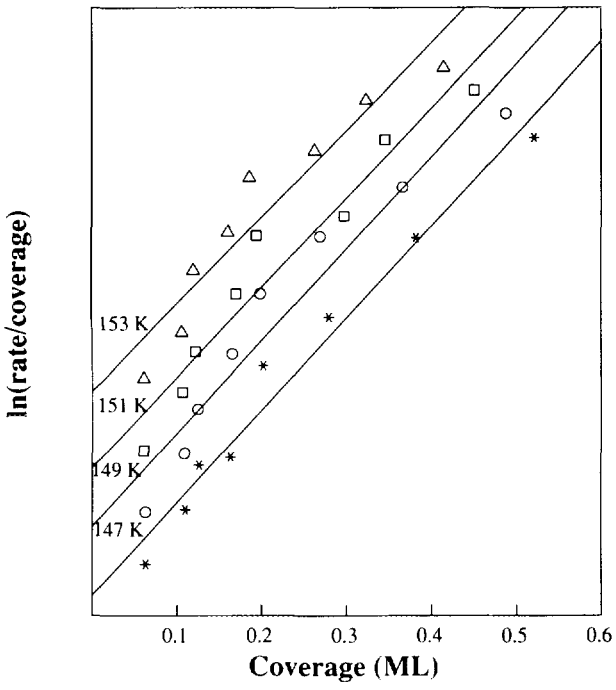

FIG. 6. Plot of propylene on Ag(110) with O(s) ln(r/coverage) as a function of coverage for temperatures 147, 149, 151, and 153 K. The slope of the isotherms is proportional to the second virial coefficient, B_2.

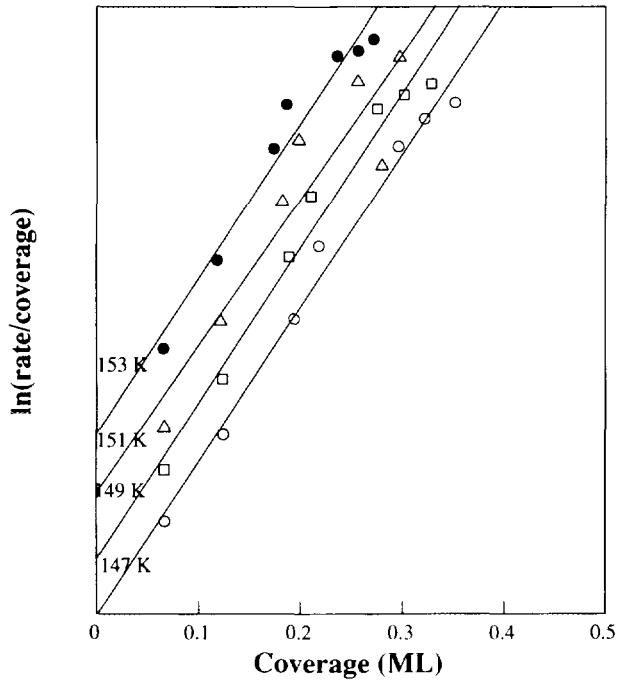

FIG. 7. Plot of propylene on Ag(110) without O(s) ln(r/coverage) as a function of coverage for temperatures 147, 149, 151, and 153 K. The slope of the isotherms is proportional to the second virial coefficient, B_2.

TABLE 2

Virial Coefficient Calculation Results

Propylene\Ag(110)	B_2 (Å^2)	Temp. range (K)	W (kcal/mol)
With O(s)	25.6 ± 2.7	147 K–155 K	−1.2 ± 0.1
Without O(s)	43.3 ± 2.54	143 K–153 K	−2.2 ± 0.2

Ag(110) atoms, q_i is the internal partition function for the gas phase molecules, Q_1 is the partition function for one adsorbed molecule and includes internal vibration as well as frustrated modes associated with localized adsorption, and Λ is the thermal wavelength, $h/(2\pi m k_b T)^{1/2}$. This expression also follows straightforwardly from simple transition state theory with the assumption that the adsorbed state can be described by the two-dimensional virial equation of state. If the virial expansion is truncated at $j = 1$, plots of $\ln(r_d/\theta)$ vs θ have a slope equal to $2B_2(N_m/A)$.

The values of B_2 averaged over the temperature ranges listed on the figures obtained from the desorption isotherms are 25.6 ± 2.7 Å^2 for Ag(110) with O(s) and 43.3 ± 2.54 Å^2 for propylene desorption from Ag(110) without O(s). A positive value of B_2 indicates repulsive interactions, whereas a negative value is indicative of attractive interactions. From these B_2 values the corresponding values of W were determined using

$$W = -2B_2(N_m/\theta)RT. \quad [3]$$

The lateral interaction energies calculated from Eq. 3 are −1.2 ± 0.1 kcal/mol and −2.2 ± 0.2 kcal/mol for the system with and without O(s), respectively; the difference is minimal. These results indicate that the lateral interaction energy does not vary significantly with and without O(s), and that the lateral interaction energy is small on both surfaces.

4. DISCUSSION

The activation energy for desorption of propylene on Ag(110) decreases slightly as the propylene coverage increases for both Ag(110) with and without O(s). In other work (18, 20) we have determined that the repulsive lateral interactions apparent in desorption originate in locally repulsive bimolecular collisions of the preferentially oriented propylene adsorbates (33). Calculations of the characteristic diffusion lengths indicate that the propylene molecules will travel large distances and experience 10^7–10^8 bimolecular collisions, thus establishing quasi-equilibrium before they desorb (18, 32). Consequently, the repulsive interactions occur even at low propane cov-

erage. The repulsive interactions between adsorbed propylene molecules appear to originate in forces exerted in a bimolecular encounter on the surface which distort the alkene from its preferred bonding orientation. These forces steepen the repulsive portion of the intermolecular potential, compared to that expected for simple physical adsorption. These interactions are thus reflected in the two-dimensional equation of state of the adsorbed alkene, and they have the effect of destabilizing the species toward desorption.

The results in this study indicate that subsurface oxygen does not affect the electron density of the silver surface atoms in such a way as to alter the binding energy of the propylene–Ag bond. These observations are in agreement with a previous study which concluded that O(s) does not influence the orientation of chemisorbed molecular oxygen on Ag(110) (5) and with studies that suggest that subsurface oxygen does not promote the ethylene epoxidation reaction (4). It appears that O(s) does not affect the reactivity or bonding of silver at the surface in a manner analogous to chemisorbed atomic oxygen. There is, for example, no indication of the creation of Lewis acid sites by O(s). Although surface oxygen creates Lewis acid sites for adsorption, the interaction with subsurface oxygen may be screened by silver atoms at the surface.

6. CONCLUSION

TPD and XPS results show that subsurface oxygen does not affect the activation energy, preexponential factor, or lateral interaction energy of π-bonded propylene on Ag(110); Lewis acid sites similar to those created by chemisorbed atomic oxygen are not observed.

ACKNOWLEDGMENT

The authors gratefully acknowledge the support of the National Science Foundation (NSF CTS 9300188-A1), without which this work could not have been accomplished.

REFERENCES

1. Van Santen, R. A., and de Groot, C. P. M., *J. Catal.* **98,** 530 (1986).
2. Grant, R. B., and Lambert, R. M., *J. Catal.* **92,** 364 (1985).
3. Van den Hoek, P. J., and Baerends, E. J., *Surf. Sci.* **221** (1989).
4. Campbell, C. T., and Paffett, M. T., *Surf. Sci.* **143** (1984) 517.
5. Pawela-Crew, J., and Madix, R. J., *Surf. Sci.*, submitted for publication (1994).
6. Barteau, M. A., and Madix, R. J., *J. Am. Chem. Soc.* **105** (1983), 344.
7. Barteau, M. A., Bowker, M., and Madix, R. J., *Surf. Sci.* **94,** 303 (1980).
8. Barteau, M. A., Bowker, M., and Madix, R. J., *J. Catal.* **67,** 118 (1981).
9. Wachs, I. E., and Madix, R. J., *J. Catal.* **53,** 208 (1978).
10. Barteau, M. A., and Madix, R. J., "Principles," (D. A. King, and D. P. Woodruff, Eds.), Vol. 4. Elsevier, New York, 1983.
11. Roberts, J. T., Madix, R. J., and Crew, W. W., *J. Catal.* **141,** 300 (1993).
12. Hawker, S., Mukoid, C., and Badyal, J. P. S., *Surf. Sci.* **219,** L615 (1989).
13. Roberts, J. T., and Madix, R. J., *J. Am. Chem. Soc.* **110,** 8540 (1988).
14. Elliot, G. S., Wu, K., and Kevan, S., *Phys. Rev. Lett.* **66,** 433 (1991).
15. Peterson, L. D., and Kevan, S. D., *Phys. Rev. Lett.* **65,** 2563 (1990).
16. Wu, K. J., and Kevan, S. D., *J. Chem. Phys.* **95,** 5355 (1991).
17. Christmann, K., *Mol. Phys.* **66,** 1 (1989).
18. Solomon, J. L., and Madix, R. J., *J. Chem. Phys.* **94,** 12 (1991).
19. Wagner, C. D., Riggs, W. M., Davis, L. E., and Moulder, J. F., "Handbook of X-Ray Photoelectron Spectroscopy." Perkin Elmer, Eden Prairie, MN, 1979.
20. Pawela-Crew, J., and Madix, R. J., *J. Chem. Phys.*, submitted for publication (1994).
21. Solomon, J. L., Ph.D. thesis. Stanford University, 1990.
22. Niemantsverdriet, J. W., and Jong, A. M., *Surf. Sci.* **233,** 365 (1991).
23. Habenschaden, E., and Kuppers, J., *Surf. Sci.* **138,** L147 (1984).
24. Barteau, M. A., and Madix, R. J., *Surf. Sci.* **97,** 101 (1980).
25. Joyner, R. W., and Roberts, M. W., *Chem. Phys. Lett.* **60,** 460 (1979).
26. McCarty, J. G., and Madix, R. J., *J. Catal.* **48,** 422 (1977).
27. Barteau, M. A., and Madix, R. J., *Surf. Sci.* **97,** 101 (1980).
28. Campbell, C. T., and Paffett, M. T., *Surf. Sci.* **143,** 517 (1984).
29. Engelhardt, H. A., and Menzel, D., *Surf. Sci.* **57,** 591 (1976).
30. Falconer, J. L., and Madix, R. J., *Surf. Sci.* **48,** 393 (1975).
31. Redhead, P. A., *Vacuum* **12,** 203 (1962).
32. Pawela-Crew, J., and Madix, R. J., *Surf. Sci.*, submitted for publication (1994).
33. Solomon, J. L., Madix, R. J., and Stöhr, J., *J. Chem. Phys.* **93,** 8379 (1990).